Progress In Electromagnetics Research, Vol. 123, 205–225, 2012

A HYBRID NFM/MOM FULL-WAVE ANALYSIS OF LAYERED PROLATE HEAD MODEL EXPOSED TO HANDSET ANTENNA

L. Zhao[1, 3, *] and K.-L. Wu[2]

[1]Center for Computational Science and Engineering, School of Mathematical Sciences, Xuzhou Normal University, China

[2]Department of Electronic Engineering, The Chinese University of Hong Kong, Shatin, Hong Kong, China

[3]State Key Laboratory of Millimeter Waves, Southeast University, China

Abstract—The electromagnetic radiation of a handset antenna to a human head model is rigorously analyzed by a new hybrid approach. In the analysis, human head is modeled by a double layered prolate spheroid with complex permittivity. A hybrid Null Field Method/Method of Moments (NFM/MoM) approach is proposed for the first time. The method is general and capable of dealing with multiple scatterers and radiators. By means of the hybrid approach, the NFM is used to model the scattering problem of the head model, and the MoM is applied to a handset antenna. The electromagnetic coupling between the head model and an antenna is taken into account by a fast convergent iteration process. Numerical results of electric field near and inside the head model and the input impedance of the antenna are calculated by the proposed hybrid approach and commercial full wave EM software. Very good agreement is obtained, which demonstrates the accuracy and efficiency of the proposed approach.

Received 8 November 2011, Accepted 15 December 2011, Scheduled 20 December 2011

* Corresponding author: Lei Zhao (lzhaomax@163.com).

1. INTRODUCTION

The radiation of electromagnetic (EM) wave to human body has been continuously raising public concerns regarding potential health issues. The concerns arouse great interest in studying the interactions between a handset antenna and human head. Most of countries in the world have adopted international safety guideline and exposure limits, including IEEE Std 1528-2003 and IEC 62209-1. The peak spatial average specific absorption rate (SAR), which is based on the electric field distribution within the exposed body, is a key index for such exposure [1, 2]. In order to assess the SAR value of a mobile phone, a semi-open phantom filled with tissue-equivalent liquid is generally employed to mimic human head, and a 3-dimensional electric field distribution is scanned within the phantom by a high precision robotic arm. The measurement procedure is very time-consuming (usually more than 90 minutes per channel and about 4 to 6 hours per a GSM phone), and the required high precision robotic arm is prohibitively expensive for its popular use in mobile phone industry. To alleviate the predicaments, the computational methods for assessing the SAR have also drawn a great deal of attention by international standard bodies, such as IEEE Standards Coordinating Committees 34 and 28 (ICES), by which the well-established Finite Difference Time Domain (FD-TD) method is an accepted assessment scheme.

In addition to a rigorous and accurate electromagnetic simulation, which usually either takes long computing hours or requires a very powerful computer resource, a very fast and low-cost computational model for a quick estimation of SAR value is also highly demanded by mobile phone antenna design engineers. As far as the computer electromagnetic simulation is concerned, people always look for an efficient solution for the electromagnetic problem which consists of a legitimate human head model and a mobile phone antenna. Some analytical and semi-analytical techniques have been used to analyze the problem from homogeneous or multilayered spherical head model exposed to EM radiation [3–5]. However, the interaction between the head model and the antenna is not taken into account in [3, 4]. In [5], the Green's function for a layered sphere obtained by superposition of spherical harmonic functions and the method of auxiliary sources (MAS) are employed to model the interaction between the layered sphere head model and a dipole antenna. It is very difficult to extend the method to a non-spherical shaped head model, such as a layered prolate. The Method of Moment (MoM) [6] and FD-TD [7–10] algorithms are widely used for analyzing such a problem. Although MoM is versatile for modeling electrically small metallic

antennas, for an electrically large inhomogeneous dielectric object, such as a human head model, the MoM needs to deal with a large number of unknowns and requires very long simulation time. Other pure numerical approaches, such as FD-TD, also require tremendous computer resources and take long time to give a satisfactory convergent solution.

In addition to numerical methods, various hybrid approaches have also been proposed to combine the strength of different numerical techniques. For example, a hybrid finite-element method (FEM)/MoM technique was developed for SAR calculations in a human phantom exposed to a base-station antenna [11], in which the advantage of integral equation approach of MoM is combined with that of the differential equation approach of FEM. Similarly, a hybrid technique of FD-TD and MoM was also developed for calculating the electromagnetic fields in a head model [12–15]. As the scattering problem of the head model must be solved in each iteration [16], long simulation time is inevitable.

The Null Field Method (NFM) developed by Watermam [17–19] is considered as an efficient analytical tool for analyzing electromagnetic scattering problem consisting of dielectric objects. Since early 1980s, a number of modifications to the NFM have been proposed, especially to improve the numerical stability in computations for dielectric objects with extreme geometries and multilayered objects [20–27]. Due to its natural of analytical treatment and its use of spherical harmonic functions as entire domain base functions, the NFM has exhibited a great deal of attraction in terms of the computational efficiency and the accuracy for many scattering problems comprising dielectric objects with canonical shapes.

In this paper, a new hybrid method of NFM and MoM is proposed for analyzing the electromagnetic problem. The hybrid method takes the advantage of high computational efficiency of the NFM for a composite dielectric object with high complex permittivity and the versatility of the MoM in modeling an electrically small metallic antenna. Therefore, the new approach leads to a highly efficient and versatile solution to the electromagnetic radiation problem of a handset antenna in the vicinity of a layered prolate head model. A remarkable feature of this hybrid solution is that the two small dimension matrices need to be inversed only once in the iteration process, which leads to a fast iterative solution solved separately in two computational domains. Having said that, with a pre-calculated system function (the inverse of the matrix) for the prolate head model, a small MoM problem needs to be solved when the antenna configuration is modified. This attribute allows a nearly real-time SAR estimation in the design stage

of a handset antenna.

2. THEORY AND METHOD

In the proposed method, the problem is divided into two segregated computational regions: the source region and scatterer region as depicted in Figure 1. The source region is defined by the antenna and is solved by the MoM, whereas the scatterer region consists of the head model and the NFM is used to solve the near field scattering problem. An iterative procedure is used to incorporate the coupling of the two regions. In the iteration process, the induced current in the source region is solved with the excitations of the original source applied to the antenna and the scattered field by the scatterer region as the secondary source. In this case, the induced currents in the scatterer region are used to compute the scattered fields on the surface of the source region. These two analyses will be alternatively repeated until the solution is converged.

2.1. MoM Modeling for Source Region

The hybrid method starts from calculating the induced surface current in the source region. For a metal strip antenna in free space, the surface currents $\bar{J}$ are expanded by Rao-Wilton-Glisson (RWG) basis functions in the form of

$$\bar{J} = \sum_{n=1}^{N_{\mathrm{MoM}}} I_n \Lambda_n \tag{1}$$

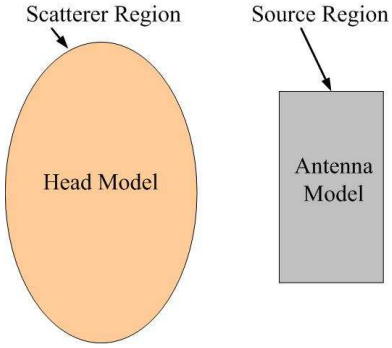

Figure 1. Geometry model of NFM scatter region and MoM source region.

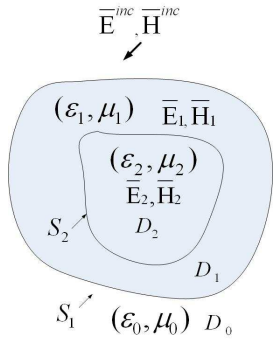

Figure 2. Scattering problem of a double-layered dielectric object.

where $\{\Lambda_n\}_{n=1}^{N_{\text{MoM}}}$ are the RWG basic functions [6] and N_{MoM} is the total number of unknowns in the source region. By applying the MoM, one can obtain an $N_{\text{MoM}} \times N_{\text{MoM}}$ linear equations with unknown current coefficients $\{I_n\}$ as

$$\bar{Z} \cdot \bar{I} = \bar{V} \tag{2}$$

To account for the primary voltage source, the so-called delta function generator is used [28]. Supposing the voltage generator is associated with cell m whose edge length is l_m, all the entries in the voltage vector $\bar{V}$ in (2) will be zero except element m whose value $V_m = l_m V$, where V is the voltage applied at the source gap. The induced currents can be obtained by solving matrix Equation (2). The antenna impedance is then calculated by

$$Z_A = \frac{V_m}{l_m^2 I_m} \tag{3}$$

2.2. NFM Modeling of Head Model

Consider the EM scattering problem of a double layered dielectric object with permittivity and permeability (ε_1, μ_1) in the shell layer and (ε_2, μ_2) in the core, respectively, which resides in free space characterized by (ε_0, μ_0) as shown in Figure 2. According to the equivalence principle [29], the problem can be solved by considering two simpler equivalent problems, an internal equivalent problem and an external equivalent problem as shown in Figure 3.

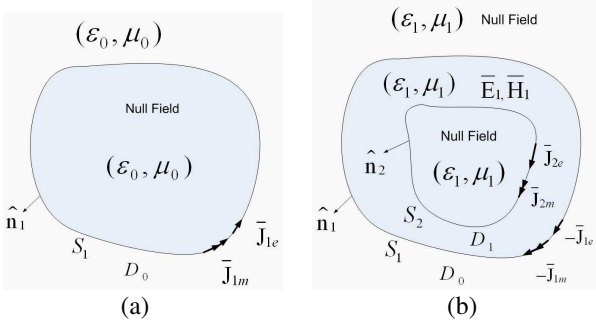

Figure 3. Equivalent problems in null field method. (a) External equivalence. (b) Internal equivalence.

2.2.1. Surface Current Approximations

In the application of the NFM, the surface currents are approximated by a linear superposition of a finite set of vector spherical wave

functions (VSWF's). Taking into account the completeness property of the regular and radiating vector spherical wave functions on enclosing surfaces, the surface magnetic and electric currents on S_1 can be approximated by a finite expansion as [25]:

$$\begin{aligned}\begin{pmatrix} \bar{J}_{1m}(\bar{r}') \\ \bar{J}_{1e}(\bar{r}') \end{pmatrix} = & \sum_{\mu=1}^{N} c_{1\mu}^{N} \begin{pmatrix} -\hat{n}_1(\bar{r}') \times \bar{M}_{\mu}^{1}(k_1\bar{r}') \\ -i\sqrt{\frac{\varepsilon_1}{\mu_1}}\hat{n}_1(\bar{r}') \times \bar{N}_{\mu}^{1}(k_1\bar{r}') \end{pmatrix} \\ & + d_{1\mu}^{N} \begin{pmatrix} -\hat{n}_1(\bar{r}') \times \bar{N}_{\mu}^{1}(k_1\bar{r}') \\ -i\sqrt{\frac{\varepsilon_1}{\mu_1}}\hat{n}_1(\bar{r}') \times \bar{M}_{\mu}^{1}(k_1\bar{r}') \end{pmatrix} \\ & + \tilde{c}_{1\mu}^{N} \begin{pmatrix} -\hat{n}_1(\bar{r}') \times \bar{M}_{\mu}^{2}(k_1\bar{r}') \\ -i\sqrt{\frac{\varepsilon_1}{\mu_1}}\hat{n}_1(\bar{r}') \times \bar{N}_{\mu}^{2}(k_1\bar{r}') \end{pmatrix} \\ & + \tilde{d}_{1\mu}^{N} \begin{pmatrix} -\hat{n}_1(\bar{r}') \times \bar{N}_{\mu}^{2}(k_1\bar{r}') \\ -i\sqrt{\frac{\varepsilon_1}{\mu_1}}\hat{n}_1(\bar{r}') \times \bar{M}_{\mu}^{2}(k_1\bar{r}') \end{pmatrix} \end{aligned} \tag{4}$$

where

$$\begin{aligned} \bar{J}_{1e} &= \hat{n}_1 \times \bar{H}_1 \quad \text{on } S_1 \\ \bar{J}_{1m} &= -\hat{n}_1 \times \bar{E}_1 \quad \text{on } S_1 \end{aligned} \tag{5}$$

are the equivalent electric current and magnetic current on surface S_1, respectively. N is a truncation number of combined index μ, $\mu = 1, 2, \ldots, N$ when $n = 1, 2, \ldots, N_{\text{rank}}$, $m = -n, \ldots, n$ and N_{rank} is the maximum expansion order of azimuthal modes. The surface currents $\bar{J}_{2m}$, $\bar{J}_{2e}$ on S_2 are approximated by linear combinations of regular vector spherical wave functions [25]:

$$\begin{aligned}\begin{pmatrix} \bar{J}_{2m}(\bar{r}') \\ \bar{J}_{2e}(\bar{r}') \end{pmatrix} = & \sum_{\mu=1}^{N} c_{2\mu}^{N} \begin{pmatrix} -\hat{n}_2(\bar{r}') \times \bar{M}_{\mu}^{1}(k_2\bar{r}') \\ -i\sqrt{\frac{\varepsilon_2}{\mu_2}}\hat{n}_2(\bar{r}') \times \bar{N}_{\mu}^{1}(k_2\bar{r}') \end{pmatrix} \\ & + d_{2\mu}^{N} \begin{pmatrix} -\hat{n}_2(\bar{r}') \times \bar{N}_{\mu}^{1}(k_2\bar{r}') \\ -i\sqrt{\frac{\varepsilon_2}{\mu_2}}\hat{n}_2(\bar{r}') \times \bar{M}_{\mu}^{1}(k_2\bar{r}') \end{pmatrix} \end{aligned} \tag{6}$$

where

$$\begin{aligned} \bar{J}_{2e} &= \hat{n}_2 \times \bar{H}_2 \quad \text{on } S_2 \\ \bar{J}_{2m} &= -\hat{n}_2 \times \bar{E}_2 \quad \text{on } S_2 \end{aligned} \tag{7}$$

The coefficients $c_{1\mu}^{N}$, $d_{1\mu}^{N}$, $\tilde{c}_{1\mu}^{N}$, $\tilde{d}_{1\mu}^{N}$, $c_{2\mu}^{N}$, and $d_{2\mu}^{N}$ are the unknown coefficients to be determined. In the above current expansions, the

VSWF's are defined by

$$\begin{aligned}
\bar{L}^p_{nm}(k\bar{r}) &= \frac{\gamma'_{nm}}{k}\nabla\left[\psi_{nm}(kr,\theta,\phi)\right] \\
\bar{M}^p_{nm}(k\bar{r}) &= \gamma_{nm}\nabla\times\left[\bar{r}\psi_{nm}(kr,\theta,\phi)\right] \\
\bar{N}^p_{nm}(k\bar{r}) &= \frac{1}{k}\nabla\times\bar{M}^p_{nm}(kr,\theta,\phi)
\end{aligned} \tag{8}$$

where

$$\begin{aligned}
\gamma'_{nm} &= \sqrt{\frac{(2n+1)}{4\pi}\frac{(n-m)!}{(n+m)!}} \\
\gamma_{nm} &= \sqrt{\frac{(2n+1)}{4\pi n(n+1)}\frac{(n-m)!}{(n+m)!}} \\
\psi_{nm}(kr,\theta,\phi) &= z^p_n(kr)P^m_n(\cos\theta)e^{im\varphi}
\end{aligned} \tag{9}$$

in which $z^1_n(kr) = j_n(kr)$, $z^2_n(kr) = h^1_n(kr)$ are the spherical Bessel function and spherical Hankel function of the first kind, respectively. $P^m_n(\cos\theta)$ are the associated Legendre functions. The above vector spherical wave functions satisfy the vector Helmholtz wave equation.

2.2.2. Null Field Condition for the External Equivalence

According to the field equivalence theorem, in the external equivalence problem, the dielectric object is replaced by an equivalent surface current with densities of $\bar{J}_{1m}$ and $\bar{J}_{1e}$ residing on surface S_1. The whole space is now characterized by the parameters (ε_0, μ_0) and the impressed source of the incident fields ($\bar{E}^{inc}$, $\bar{H}^{inc}$). It is assumed that the total field at any point external to the surface S_1 is the same as the total field in the original problem and that the total field at any point internal to the surface S_1 is null. In other words, the incident field plus the field produced by the surface currents $\bar{J}_{1m}$ and $\bar{J}_{1e}$ radiating in the unbounded medium, give the correct total field in the external region. However, the scattered field cancels the incident field in the internal region, namely

$$\begin{aligned}
&\nabla\times\int_{S_1}(-\bar{J}_{1m})\cdot\bar{\bar{G}}(k_0,\bar{r},\bar{r}')ds' \\
&+\frac{i}{\omega\varepsilon_0}\nabla\times\nabla\times\int_{S_1}(-\bar{J}_{1e})\cdot\bar{\bar{G}}(k_0,\bar{r},\bar{r}')ds' = -\bar{E}^{inc} \\
&\bar{r}\in D_{in}\triangleq D_1\cup D_2\cup S_2
\end{aligned} \tag{10}$$

where $\bar{\bar{G}}(k, \bar{r}, \bar{r}')$ is the dyadic Green's function for a uniform infinite medium with wave number k of the region, and

$$\bar{\bar{G}}(k, \bar{r}, \bar{r}') = \frac{e^{ik|\bar{r}-\bar{r}'|}}{4\pi\,|\bar{r}-\bar{r}'|}\bar{\bar{I}} \tag{11}$$

in which $\bar{\bar{I}}$ is the identity dyadic.

2.2.3. Null Field Condition for the Internal Equivalence

In the internal equivalence, the whole space is characterized by the parameters (ε_1, μ_1). The impressed source of the incident field ($\bar{E}^{inc}$, $\bar{H}^{inc}$) has been removed and the equivalent surface currents ($-\bar{J}_{1m}$, $-\bar{J}_{1e}$) and ($\bar{J}_{2m}$, $\bar{J}_{2e}$) are placed on S_1 and S_2, respectively. These currents, radiating into the unbounded dielectric object, produce the correct total field ($\bar{E}_1$, $\bar{H}_1$) in the region bounded by the surface S_1 and S_2, and null field outside the region. Hence

$$\begin{aligned}
&-\nabla\times\int_{S_1}(-\bar{J}_{1m})\cdot\bar{\bar{G}}(k_1,\bar{r},\bar{r}')ds' - \frac{i}{\omega\varepsilon_1}\nabla\times\nabla\times\int_{S_1}\bar{J}_{1e}\cdot\bar{\bar{G}}(k_1,\bar{r},\bar{r}')ds' \\
&+\nabla\times\int_{S_2}(-\bar{J}_{2m})\cdot\bar{\bar{G}}(k_1,\bar{r},\bar{r}')ds' + \frac{i}{\omega\varepsilon_1}\nabla\times\nabla\times\int_{S_2}\bar{J}_{2e}\cdot\bar{\bar{G}}(k_1,\bar{r},\bar{r}')ds' = 0, \\
&\qquad\qquad \bar{r}\in D_0\cup D_2
\end{aligned} \tag{12}$$

2.2.4. Transformation to Linear System of Equations

In order to obtain a system of linear algebraic equations from integral equations of (10) and (12), the dyadic Green's function for an unbounded homogeneous medium is expanded with the VSWF's [30] as

$$\bar{\bar{G}}(k,\bar{r},\bar{r}') = ik\sum_{n=0}^{\infty}\sum_{m=-n}^{n}(-1)^m \left\{ \begin{array}{l} \bar{M}^{(3-p)}_{n(-m)}(k\bar{r}')\bar{M}^{p}_{nm}(k\bar{r}) \\ +\bar{N}^{(3-p)}_{n(-m)}(k\bar{r}')\bar{N}^{p}_{nm}(k\bar{r}) \\ +\bar{L}^{(3-p)}_{n(-m)}(k\bar{r}')\bar{L}^{p}_{nm}(k\bar{r}) \end{array} \right\} \tag{13}$$

where

$$p = \left\{ \begin{array}{ll} 1, & |\bar{r}| < |\bar{r}'| \\ 2, & |\bar{r}| > |\bar{r}'| \end{array} \right. \tag{14}$$

Take a note that the functions $\bar{L}^{p}_{nm}$ are irrotational, i.e., $\nabla\times\bar{L}^{p}_{nm} = 0$. Thus, these functions will not present in the final expressions because they become zero with the curl operations of (10) and (12).

The vector spherical wave expansion of the incident field can be expressed by

$$\bar{E}^{inc} = \sum_{n=1}^{\infty} \sum_{m=-n}^{n} \left\{ a_{nm} \bar{M}_{nm}^{1}(k_0 \bar{r}) + b_{nm} \bar{N}_{nm}^{1}(k_0 \bar{r}) \right\} \tag{15}$$

where coefficients a_{nm} and b_{nm} can be obtained for a given source current distribution.

Considering the general null field Equation (10), when field position vector $\bar{r}$ lies on a spherical surface inscribed in S_1, by using the expansion of the incident field and the dyad Green's function, as well as the orthogonality of the VSWF's on a spherical surface, one can obtain the following equation:

$$ik_0^2 \int_{S_1} \left[-\bar{J}_{1m} \cdot \begin{pmatrix} \bar{N}_{\bar{\upsilon}}^{2}(k_0 \bar{r}') \\ \bar{M}_{\bar{\upsilon}}^{2}(k_0 \bar{r}') \end{pmatrix} + i \sqrt{\frac{\varepsilon_0}{\mu_0}} \bar{J}_{1e} \cdot \begin{pmatrix} \bar{M}_{\bar{\upsilon}}^{2}(k_0 \bar{r}') \\ \bar{N}_{\bar{\upsilon}}^{2}(k_0 \bar{r}') \end{pmatrix} \right] ds' = - \begin{pmatrix} a_{\upsilon} \\ b_{\upsilon} \end{pmatrix}, \quad \upsilon = 1, 2, \ldots \tag{16}$$

where $\bar{\upsilon} = (n, -m)$ is a combined index.

For the general null-field Equation (12) in D_0, the same procedure can be proceed with $\bar{r}$ restricted to lying on a sphere enclosing D_0, that is

$$\begin{aligned} &-ik_1^2 \int_{S_1} \left[-\bar{J}_{1m} \cdot \begin{pmatrix} \bar{N}_{\bar{\upsilon}}^{1}(k_1 \bar{r}') \\ \bar{M}_{\bar{\upsilon}}^{1}(k_1 \bar{r}') \end{pmatrix} + i \sqrt{\frac{\varepsilon_1}{\mu_1}} \bar{J}_{1e} \cdot \begin{pmatrix} \bar{M}_{\bar{\upsilon}}^{1}(k_0 \bar{r}') \\ \bar{N}_{\bar{\upsilon}}^{1}(k_0 \bar{r}') \end{pmatrix} \right] ds' \\ &+ik_1^2 \int_{S_2} \left[-\bar{J}_{2m} \cdot \begin{pmatrix} \bar{N}_{\bar{\upsilon}}^{1}(k_1 \bar{r}') \\ \bar{M}_{\bar{\upsilon}}^{1}(k_1 \bar{r}') \end{pmatrix} + i \sqrt{\frac{\varepsilon_1}{\mu_1}} \bar{J}_{2e} \cdot \begin{pmatrix} \bar{M}_{\bar{\upsilon}}^{1}(k_0 \bar{r}') \\ \bar{N}_{\bar{\upsilon}}^{1}(k_0 \bar{r}') \end{pmatrix} \right] ds' = 0, \quad \upsilon = 1, 2, \ldots \end{aligned} \tag{17}$$

Finally, for the general null-field Equation (12) in D_2 with restriction $\bar{r}$ to lying on a sphere enclosed in D_2, there is

$$\begin{aligned} &-ik_1^2 \int_{S_1} \left[-\bar{J}_{1m} \cdot \begin{pmatrix} \bar{N}_{\bar{\upsilon}}^{2}(k_1 \bar{r}') \\ \bar{M}_{\bar{\upsilon}}^{2}(k_1 \bar{r}') \end{pmatrix} + i \sqrt{\frac{\varepsilon_1}{\mu_1}} \bar{J}_{1e} \cdot \begin{pmatrix} \bar{M}_{\bar{\upsilon}}^{2}(k_0 \bar{r}') \\ \bar{N}_{\bar{\upsilon}}^{2}(k_0 \bar{r}') \end{pmatrix} \right] ds' \\ &+ik_1^2 \int_{S_2} \left[-\bar{J}_{2m} \cdot \begin{pmatrix} \bar{N}_{\bar{\upsilon}}^{2}(k_1 \bar{r}') \\ \bar{M}_{\bar{\upsilon}}^{2}(k_1 \bar{r}') \end{pmatrix} + i \sqrt{\frac{\varepsilon_1}{\mu_1}} \bar{J}_{2e} \cdot \begin{pmatrix} \bar{M}_{\bar{\upsilon}}^{2}(k_0 \bar{r}') \\ \bar{N}_{\bar{\upsilon}}^{2}(k_0 \bar{r}') \end{pmatrix} \right] ds' = 0, \quad \upsilon = 1, 2, \ldots \end{aligned} \tag{18}$$

Inserting the current expansions in (4) and (6) into null field Equations (16)–(18), one can obtain the following system of matrix equations

$$\bar{Q}_1^{21}(k_0, k_1) \bar{i}_1 + \bar{Q}_1^{22}(k_0, k_1) \tilde{i}_1 = -\bar{e} \tag{19}$$

$$-\tilde{i}_1 + \bar{Q}_2^{11}(k_1, k_2) \bar{i}_2 = 0 \tag{20}$$

$$\bar{i}_1 + \bar{Q}_2^{21}(k_1, k_2) \bar{i}_2 = 0 \tag{21}$$

where $\bar{i}_1 = [c_{1\mu}^N, d_{1\mu}^N]^T$, $\tilde{i}_1 = [\tilde{c}_{1\mu}^N, \tilde{d}_{1\mu}^N]^T$, $\bar{i}_2 = [c_{2\mu}^N, d_{2\mu}^N]^T$, and as before, $\bar{e} = [a_\nu, b_\nu]^T$ is the vector containing the expansion coefficients of incident field. Solving the system of matrix equations, the unknown coefficients $\bar{i}_1$, $\tilde{i}_1$, and $\bar{i}_2$ can be obtained. The detailed expressions of $\bar{Q}_t^{pq}(k_1, k_2)$ matrix appearing in (19)–(21) are given in the Appendix.

2.2.5. Iteration Processing Combining NFM and MoM

The iteration process starts with applying the MoM to the source region to obtain the currents $\bar{J}$ on the antenna (assuming the primary source is applied). The scattered fields $\bar{E}_{\text{MoM}}^S$ produced by the current on the antenna surface, which are treated as the source in the NFM domain, can then be found by

$$\bar{E}_{\text{MoM}}^S = i\omega\mu \int_{S_A} \bar{\bar{G}}_0(\bar{r}, \bar{r}') \cdot \bar{J}(\bar{r}')ds' \tag{22}$$

where S_A is the surface of the antenna, and $\bar{\bar{G}}_0(\bar{r}, \bar{r}') = (\bar{\bar{I}} + \frac{\nabla\nabla}{k_0^2})g(\bar{r}, \bar{r}')$ is a dyadic Green's function in free space. Using the expansion of the dyadic Green's function $\bar{\bar{G}}$ in (13), $\bar{\bar{G}}_0$ can be rewritten as,

$$\bar{\bar{G}}_0(\bar{r}, \bar{r}') = ik_0 \sum_{n=1}^{\infty} \sum_{m=-n}^{n} (-1)^m \begin{Bmatrix} \bar{M}_{n(-m)}^{(3-p)}(k_0\bar{r}')\bar{M}_{nm}^p(k_0\bar{r}) \\ +\bar{N}_{n(-m)}^{(3-p)}(k_0\bar{r}')\bar{N}_{nm}^p(k_0\bar{r}) \end{Bmatrix} \tag{23}$$

Then, the scattered field from the antenna surface currents can be expressed with VSWF's as

$$\bar{E}_{\text{MoM}}^S = \sum_{\nu=1}^{N} \left\{ a_\nu \bar{M}_\nu^2(k_0\bar{r}) + b_\nu \bar{N}_\nu^2(k_0\bar{r}) \right\} \tag{24}$$

where

$$\begin{pmatrix} a_\nu \\ b_\nu \end{pmatrix} = -\eta_0 k_0^2 \int_{S_A} \begin{pmatrix} \bar{M}_\nu^1(k_0\bar{r}') \\ \bar{N}_\nu^1(k_0\bar{r}') \end{pmatrix} \cdot \bar{J}(\bar{r}')ds' \tag{25}$$

are the expansion coefficients of incident field for NFM region (induced by current $\bar{J}$).

The resultant null field equations for a double-layered dielectric object are given in (19)–(21) by applying the VSWF's expansions (4) and (6). The equivalent currents on the surface of the dielectric object can be obtained by solving the system of matrix Equations (19)–(21). The scattered fields $\bar{E}_{\text{NFM}}^S$ by the scatterer along, which represents the secondary source in the source region:

$$\bar{E}_{\text{NFM}}^S = \sum_{\nu=1}^{N} \left(f_\nu^N \bar{M}_\nu^2(k_0\bar{r}) + g_\nu^N \bar{N}_\nu^2(k_0\bar{r}) \right) \tag{26}$$

where

$$\begin{pmatrix} f_\nu^N \\ g_\nu^N \end{pmatrix} = ik_0^2 \int_{S_1} \begin{pmatrix} -\bar{J}_{1m} \cdot \begin{pmatrix} \bar{N}_{\bar{\nu}}^1(k_0\bar{r}') \\ \bar{M}_{\bar{\nu}}^1(k_0\bar{r}') \end{pmatrix} \\ +i\sqrt{\frac{\mu_0}{\varepsilon_0}}\bar{J}_{1e} \cdot \begin{pmatrix} \bar{M}_{\bar{\nu}}^1(k_0\bar{r}') \\ \bar{N}_{\bar{\nu}}^1(k_0\bar{r}') \end{pmatrix} \end{pmatrix} ds', \ \nu = 1, \ldots, N \quad (27)$$

If the observation point is outside the minimum circumscribing sphere of the head model, Equation (26) is valid for calculating the scattered field efficiently. However, in the near-zone region between the boundary of scatterer and the minimum circumscribing sphere, the scattered field can be obtained by the general integral equation as

$$\begin{aligned} \bar{E}_{\mathrm{NFM}}^S &= \nabla \times \int_{S_1} (-\bar{J}_{1m}) \cdot \bar{\bar{G}}(k_0, \bar{r}, \bar{r}')ds' \\ &\quad -\frac{i}{\omega\varepsilon_0}\nabla \times \nabla \times \int_{S_1} \bar{J}_{1e} \cdot \bar{\bar{G}}(k_0, \bar{r}, \bar{r}')ds' \end{aligned} \quad (28)$$

The expression for calculating $\bar{E}_{\mathrm{NFM}}^S$ using spherical vector harmonic wave functions can be obtained in [27].

The voltage induced by the scattered field in the source region, which represents the secondary excitation to the MoM solution, can be evaluated by

$$V_m^{add} = \int_{S_m} \Lambda_m(\bar{r}) \cdot \bar{E}_{NFM}^S(\bar{r})ds, \quad m = 1, 2, \ldots, N_{\mathrm{MoM}} \quad (29)$$

With the total excitation voltage contributed by both the original source excitation applied to the antenna and the secondary source created by the induced equivalent current in the NFM scatterer region, the MoM can be executed to find the updated currents on the surface of the antenna. The procedure will be repeated until a convergent solution of the EM problem is achieved. Be noted that in the iterative process, the matrices for describing the scatterer region and the source region only need to be inversed once. In the hybrid NFM/MoM algorithm, the residual relative error on the current $\bar{J}$ is used for convergence criterion, which is defined at the kth iteration as

$$\mathrm{error}(\bar{J}, k) = \frac{||\bar{J}^k - \bar{J}^{k-1}||}{||\bar{J}^k||} \quad (30)$$

where $\|\cdot\|$ denotes the 2-norm of a column vector.

3. NUMERICAL RESULTS AND HEAD MODEL VERIFICATION

To verify the proposed hybrid approach, two representative examples of an antenna near the head model are studied extensively. Without

losing generality, only the metal antenna models are used in the examples. The head model used is a layered dielectric prolate, whose major semi-axial lengths of outer and inner layer are 100 mm and 98 mm, respectively. The ellipticity of the prolate spheroid is 0.8. The permittivity, conductivity and mass density parameters of the dielectric layer and the core are $\varepsilon_{r1} = 5$, $\sigma_1 = 0.05\,\mathrm{S/m}$, $\rho_1 = 1000\,\mathrm{kg/m^3}$, $\varepsilon_{r2} = 42$, $\sigma_2 = 0.99\,\mathrm{S/m}$, and $\rho_2 = 1000\,\mathrm{kg/m^3}$, respectively. The EM exposure problem of human head by a handset, as shown in Figure 4, is simulated by both the proposed hybrid approach and commercial GEMS software [31] which is based on parallel FDTD [32, 33]. Both the proposed hybrid algorithm implemented with Fortran code and GEMS software are performed on a parallel processing platform installed with windows operating system which have 16 CPUs (3.0 GHz) and 32 GB memory.

3.1. The Prolate Head Model Exposed to Dipole Antenna

It is known that the accuracy of the calculated impedance value of an antenna largely depends on the accuracy of the calculated near field in a given environment. To verify the accuracy of the proposed hybrid approach, particularly the modeling of the interaction between the prolate head model and an antenna, the input impedance of a half wavelength strip dipole antenna in the vicinity of the head model, as shown in Figure 4, is investigated.

The input impedances of the dipole antenna at different distances

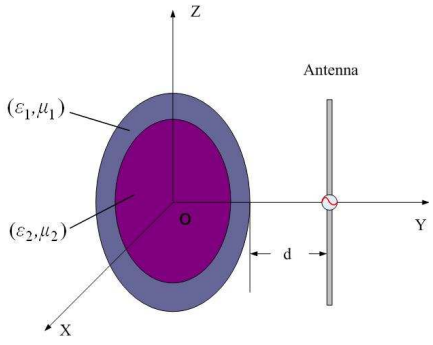

Figure 4. Geometry of the head model exposed to a dipole antenna.

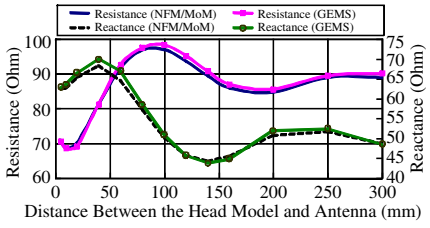

Figure 5. Input impedance of a dipole antenna adjacent to a layered prolate versus separation distance d. Operating frequency is 0.9 GHz.

away from the head model are calculated by both proposed approach and the commercial GEMS software. In the modeling by the hybrid approach, the definition of input impedance is given by Equation (3). It can be seen from Figure 5 that very good agreement between the results by the GEMS software and the proposed approach can be observed. To show the speed of convergence of the hybrid approach, the electric field intensity calculated in the first three iterations alone an observation line are compared with the full wave GEMS simulation in Figure 6. It shows that only three iterations are sufficient to obtain a convergent result. The detailed electric field across a cut-plane is calculated and is presented in Figure 7. In the simulations, the distance between the head model and the dipole antenna is set to $d = 20\,\text{mm}$ and the operating frequency is set to 900 MHz. It can be seen that the field distribution calculated by the hybrid NFM/MoM and those by the GEMS resemble very well in all the field components, which further justifies that the proposed approach can serve as an accurate

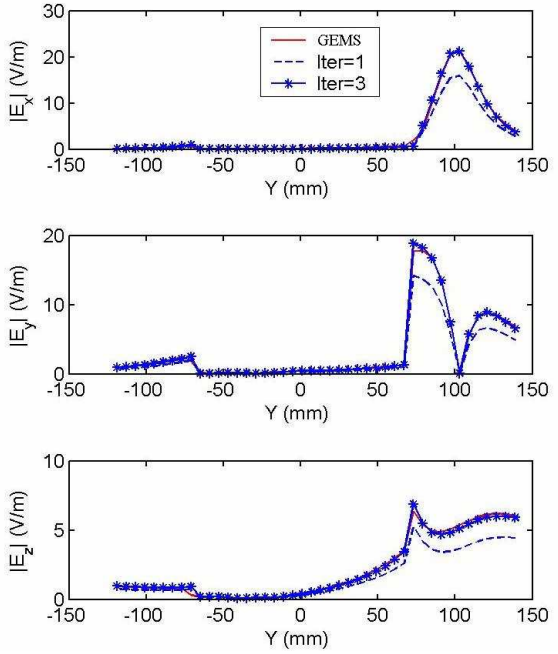

Figure 6. Field distribution on the line of $x = 20\,\text{mm}$, $z = 39\,\text{mm}$ from the prolate head model adjacent to a half wavelength dipole antenna with separation distance d of 20 mm. Number of iteration = 1 and 3, respectively.

and effective tool for calculating the electromagnetic problem.

In the NFM/MoM simulation, the half-wavelength strip dipole is divided into 388 triangles, and the expansion order N_{rank} in NFM is set to 6. The impedance matrix of the MoM and the Q matrix, which only needs to be calculated once, can be pre-calculated and stored in memory. The CPU time for each iteration is about 10 s. For the interaction problem between the prolate head model and the half-wavelength dipole antenna, the required CPU time is about 30 s using the hybrid method. However, the CPU time for the GEMS simulation is about 3,000 s on the same workstation.

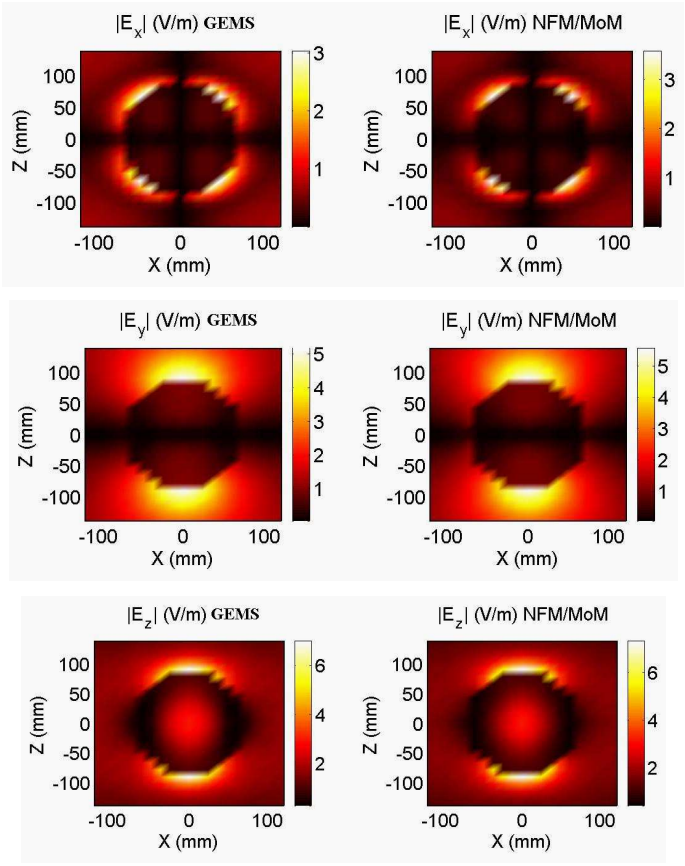

Figure 7. Field distribution on a cut-plane of $y = 40$ mm across the prolate head model adjacent to a half wavelength dipole antenna with separation distance $d = 20$ mm. Number of iterations = 3.

3.2. The Head Model Exposed to Dual Band PIFA Antenna

The SAR distribution induced by a dual-band planar inverted-F antenna (PIFA) for a handset is investigated in this example. The configuration of the antenna is shown in Figure 8. The dual-band antenna works at GSM band (900 MHz) and DCS band (1800 MHz). Figure 9 shows the calculated return loss of the PIFA antenna when it is placed in free space and near the head model. It is found, through analysis, that the resonance frequency of the PIFA antenna shifts when the antenna is closely placed to the head model by 25 MHz and 7.5 MHz downward at GSM band and DCS band, respectively.

If not specifically stated, the SAR distribution is referred to the point SAR inside the head model instead of the maximum average SAR. The reason is that the emphasis of this research is placed on the electromagnetic analysis rather than how to calculate the SAR value. With an accurate point SAR distribution available the maximum average SAR will automatically be accurate. The following definition of the point SAR value is used in this work [2]:

$$\text{SAR} = \frac{\sigma}{\rho}|\bar{E}|^2 \tag{31}$$

where σ is the electric conductivity, ρ the density of the tissue, and $\bar{E}$ the computed *rms* electric field intensity at a given frequency. Figures 10 and 11 show the SAR distribution on a cut plane when the operating frequency is 900 MHz and 1800 MHz, respectively. To demonstrate the accuracy of the internal field calculated by the hybrid approach, the SAR distribution along the center line of the cut plane is calculated by the GEMS software and the proposed hybrid method with 5 iterations. In both simulations, the prolate head model is

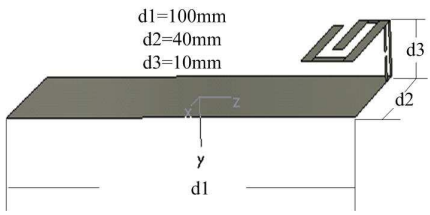

Figure 8. A dual band PIFA antenna for a handset.

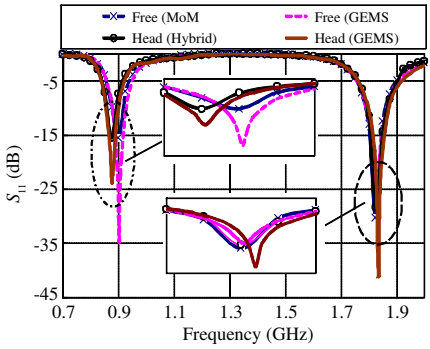

Figure 9. Return loss of the PIFA antenna.

placed 15 mm away from the dual band PIFA antenna. As shown in Figure 12, the calculated SAR using the hybrid NFM/MoM method are in very good agreement with those of the GEMS simulation. It should be mentioned that all the calculated SAR data in Figures 10–12 are normalized to 1 W radiated power from the PIFA antenna.

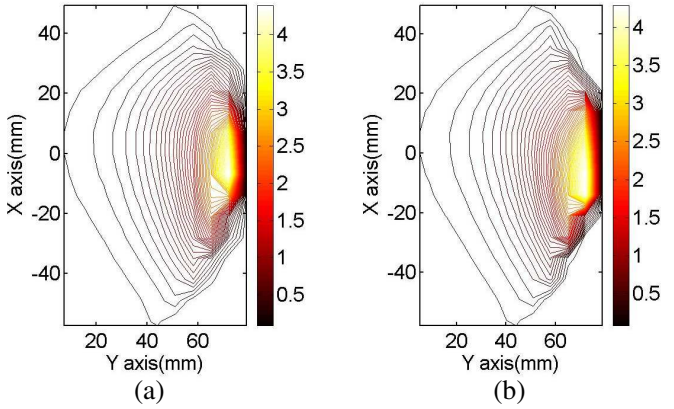

Figure 10. SAR (W/kg, normalized to 1 W radiated power) distribution on plane $z = 34$ mm. A prolate head model exposed a dual band PIFA antenna with distance $d = 15$ mm. Operating frequency is 0.9 GHz. Number of iterations = 5. (a) GEMS simulation. (b) Hybrid NFM/MoM.

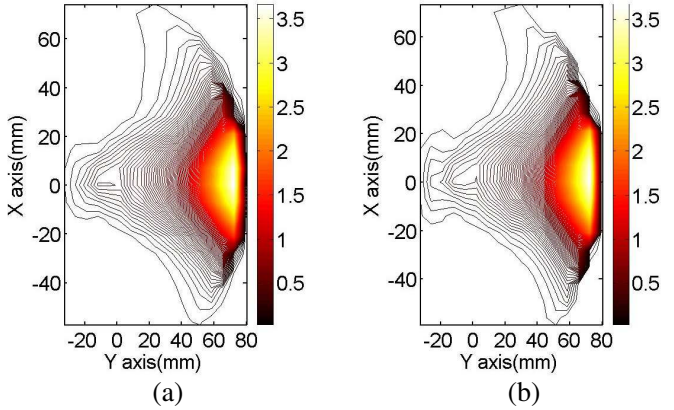

Figure 11. SAR (W/kg, normalized to 1 W radiated power) distribution on plane $z = -20$ mm. A prolate head model exposed a dual band PIFA antenna with distance $d = 15$ mm. Operating frequency is 1.8 GHz. Number of iteration = 5.

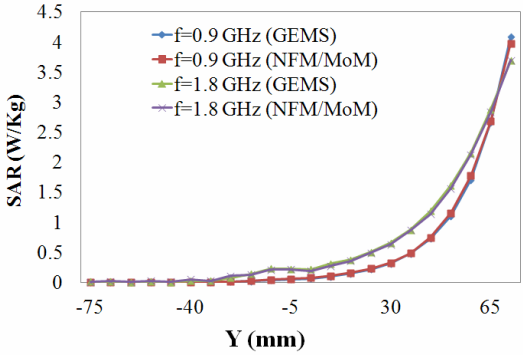

Figure 12. SAR (W/kg, normalized to 1 W radiated power) distribution along line $x = 0$, $z = 34$ mm for $f = 0.9$ GHz and along line $x = 0$, $z = -20$ mm for $f = 1.8$ GHz, when the prolate head model is exposed to a dual band PIFA antenna with 15 mm separation distance. Number of iteration = 5.

4. CONCLUSION

The EM radiation of a handset antenna operating in the vicinity of a layered prolate head model is investigated by a novel hybrid NFM/MoM simulation approach. The new hybrid approach takes into account the interaction of the antenna with the head model. The numerical MoM and analytical NFM are used to solve the antenna (source region) and the layered prolate head model (scatter region), separately, and an iteration scheme is used to combine the two different schemes that are performed in two different regions. By combining the strength of the numerical and the analytical approaches, solving the complex radiation problem becomes far more efficient than the existing pure numerical approach and is more practical than those existing analytical solutions to the concerned problem. Two practical numerical examples have shown the validation, accuracy and efficiency of the proposed hybrid method. Due to the analytical natural of the NFM, the number of unknowns in the NFM solution is very small, which makes the hybrid NFM/MoM to be very efficient. The proposed hybrid approach can be used for quick estimation of the SAR distribution induced by a mobile phone antenna.

The conventional derivation of the NFM relies on the approximation of the surface fields by the system of localized vector spherical wave functions (VSWF), which can provide a good approximation to the solution when the surface is not extremely aspherical. When this is not the case, such as SAM head model, the NFM with discrete

source can possible to extend the application rage of the single spherical coordinate-based NFM [25]. The future work include incorporating the discrete sources method in the null field method to extend the proposed hybrid approach to calculating SAR value in a head model with more realistic facial features.

APPENDIX A.

The elements of $\bar{Q}_t^{pq}(k_1, k_2)$ are given by

$$\bar{Q}_t^{pq}(k_1, k_2) = \begin{bmatrix} (Q_t^{pq})_{\nu\mu}^{11} & (Q_t^{pq})_{\nu\mu}^{12} \\ (Q_t^{pq})_{\nu\mu}^{21} & (Q_t^{pq})_{\nu\mu}^{22} \end{bmatrix} \tag{A1}$$

where

$$(Q_t^{pq})_{\nu\mu}^{11} = ik_1^2 \int_{S_t} \left\{ \begin{array}{l} [\hat{n}(\bar{r}') \times \bar{M}_\mu^q(k_2\bar{r}')] \cdot \bar{N}_\nu^p(k_1\bar{r}') \\ +\sqrt{\frac{\varepsilon_2}{\varepsilon_1}}[\hat{n}(\bar{r}') \times \bar{N}_\mu^q(k_2\bar{r}')] \cdot \bar{M}_\nu^p(k_1\bar{r}') \end{array} \right\} ds' \tag{A2}$$

$$(Q_t^{pq})_{\nu\mu}^{12} = ik_1^2 \int_{S_t} \left\{ \begin{array}{l} [\hat{n}(\bar{r}') \times \bar{N}_\mu^q(k_2\bar{r}')] \cdot \bar{N}_\nu^p(k_1\bar{r}') \\ +\sqrt{\frac{\varepsilon_2}{\varepsilon_1}}[\hat{n}(\bar{r}') \times \bar{M}_\mu^q(k_2\bar{r}')] \cdot \bar{M}_\nu^p(k_1\bar{r}') \end{array} \right\} ds' \tag{A3}$$

$$(Q_t^{pq})_{\nu\mu}^{21} = ik_1^2 \int_{S_t} \left\{ \begin{array}{l} [\hat{n}(\bar{r}') \times \bar{M}_\mu^q(k_2\bar{r}')] \cdot \bar{M}_\nu^p(k_1\bar{r}') \\ +\sqrt{\frac{\varepsilon_2}{\varepsilon_1}}[\hat{n}(\bar{r}') \times \bar{N}_\mu^q(k_2\bar{r}')] \cdot \bar{N}_\nu^p(k_1\bar{r}') \end{array} \right\} ds' \tag{A4}$$

$$(Q_t^{pq})_{\nu\mu}^{22} = ik_1^2 \int_{S_t} \left\{ \begin{array}{l} [\hat{n}(\bar{r}') \times \bar{N}_\mu^q(k_2\bar{r}')] \cdot \bar{M}_\nu^p(k_1\bar{r}') \\ +\sqrt{\frac{\varepsilon_2}{\varepsilon_1}}[\hat{n}(\bar{r}') \times \bar{M}_\mu^q(k_2\bar{r}')] \cdot \bar{N}_\nu^p(k_1\bar{r}') \end{array} \right\} ds' \tag{A5}$$

ACKNOWLEDGMENT

This work was supported in part by the Shun Hing Institute of Advanced Engineering, The Chinese University of Hong Kong, in part by the Natural Science Foundation of Jiangsu Province under Grant No. BK2010174, in part by Natural Science Foundation of the Jiangsu Higher Education Institutions under Grant No. 10KJB510025, and in part by the Open Project Program of State Key Laboratory of Millimeter Waves under Grant No. K201008.

REFERENCES

1. *Procedure to Determine the Specific Absorption Rate (SAR) for Hand-held Devices Used in Close Proximity to the Ear (Frequency Range of 300 MHz to 3 GHz)*, International Electrotechnical Commission (IEC) Standard 62209-1, Feb. 2005.
2. *IEEE Recommended Practice for Determining the Peak Spatial-average Specific Absorption Rate (SAR) in the Human Head From Wireless Communications Devices: Measurement Techniques*, IEEE Standard 1528-2003, Dec. 2003.
3. Weil, C. M., "Absorption characteristics of multilayered sphere models exposed to UHF/microwave radiation," *IEEE Trans. Biomed. Eng.*, Vol. 22, 468–476, 1975.
4. Cottis, P. G. and N. K. Uzunoglu, "Focusing properties of dipole arrays placed near a multilayer lossy sphere," *Journal of Electromagnetic Waves and Applications*, Vol. 4, No. 5, 431–440, 1990.
5. Nikita, K., G. Stamatakos, N. Uzunoglu, and A. Karafotias, "Analysis of the interaction between a layered spherical human head model and a finite-length dipole," *IEEE Trans. Microwave Theory Tech.*, Vol. 48, 2003–2013, 2000.
6. Rao, S. M., D. R. Wilton, and A. W. Glisson, "Electromagnetic scattering by surfaces of arbitrary shape," *IEEE Trans. Antennas Propag.*, Vol. 30, 409–418, 1982.
7. Dimbylow, P. J. and O. P. Gandhi, "Finite-difference time-domain calculations of SAR in a realistic heterogeneous model of the head for plane-wave exposure from 600 MHz to 3 GHz," *Phys. Med. Biol.*, Vol. 36, 1075–1089, 1991.
8. Okoniewski, M. and M. A. Stuchly, "A study of the handset antenna and human body interaction," *IEEE Trans. Microwave Theory Tech.*, Vol. 44, 1855–1864, 1996.
9. Kühn, S., W. Jennings, A. Christ, and N. Kuster, "Assessment of induced radio-frequency electromagnetic fields in various anatomical human body models," *Phys. Med. Biol.*, Vol. 54, 875–890, 2009.
10. Christ, A., A. Klingenböck, T. Samaras, C. Goiceanu, and N. Kuster, "The dependence of electromagnetic far-field absorption on body tissue composition in the frequency range from 300 MHz to 6 GHz," *IEEE Trans. Microwave Theory Tech.*, Vol. 54, 2188–2195, 2006.
11. Meyer, F. J. C., D. B. Davidson, U. Jakobus, and M. A. Stuchly, "Human exposure assessment in the near field of GSM base-

station antennas using a hybrid finite element/method of moments technique," *IEEE Trans. Biomed. Eng.*, Vol. 50, 224–233, 2003.

12. Abd-Alhameed, R. A., P. S. Excell, and M. A. Mangoud, "Computation of specific absorption rate in the human body due to base-station antennas using a hybrid formulation," *IEEE Trans. Microwave Theory Tech.*, Vol. 48, 2014–2021, 2000.
13. Mangoud, M. A., R. A. Abd-Alhameed, and P. S. Excell, "Simulation of human interaction with mobile telephones using hybrid techniques over coupled domains," *IEEE Trans. on Electromagnetic Compatibility*, Vol. 47, 374–381, 2005.
14. Cerri, G., P. Russo, A. Schiavoni, G. Tribellini, and P. Bielli, "MOM-FDTD hybrid technique for analyzing scattering problems," *Electronics Letters*, Vol. 34, 438–440, 1998.
15. Koulouridis, S. and K. S. Nikita, "Study of the coupling between human head and cellular phone helical antennas," *IEEE Trans. on Electromagnetic Compatibility*, Vol. 46, 62–70, 2004.
16. Kaye, M., P. K. Murthy, and G. A. Thiele, "An iterative method for solving scattering problem," *IEEE Trans. Antennas Propag.*, Vol. 33, 1272–1279, 1985.
17. Waterman, P. C., "Matrix formulation of electromagnetic scattering," *Proc. IEEE*, Vol. 53, 805–812, 1965.
18. Waterman, P. C., "Scattering by dielectric obstacles," *Alta Freq.*, Vol. 38, 348–352, 1969.
19. Waterman, P. C., "New formulation of acoustic scattering," *J. Acoust. Soc. Am.*, Vol. 45, 1417–1429, 1969.
20. Peterson, B. and S. Ström, "T-matrix for electromagnetic scattering from an arbitrary number of scatterers and representations of E(3)," *Phys. Rev. D*, Vol. 8, 3661–3678, 1973.
21. Ström, S. and W. Zheng, "The null field approach to electromagnetic scattering from composite objects," *IEEE Trans. Antennas Propag.*, Vol. 36, 376–382, 1988.
22. Strom, S. and W. Zheng, "Basic features of the null field method for dielectric scatterers," *Radio Science*, Vol. 22, 1273–1281, 1987.
23. Gürel, L. and W. C. Chew, "Recursive algorithms for the scattering by N disks or strips," *IEEE Trans. Antennas Propag.*, Vol. 38, 507–515, 1990.
24. Doicu, A. and T. Wriedt, "Null-field method with discrete sources to electromagnetic scattering from layered scatterers," *Comput. Phys. Commun.*, Vol. 138, 136–142, 2001.
25. Doicu, A., T. Wriedt, and Y. A. Eremin, *Light Scattering by Systems of Particles*, Springer, 2006.

26. Tsitsas, N. L., "Direct and inverse dipole electromagnetic scattering by a piecewise homogeneous sphere," *J. Applied Mathematics and Mechanics*, Vol. 89, 833–849, 2009.
27. Doicu, A. and T. Wried, "Near-field computation using the null-field method," *J. Quant. Spectrosc. Radiat. Transf.*, Vol. 111, 466–473, 2010.
28. Makarov, S., "MoM antenna simulations with matlab: RWG basis functions," *IEEE Antennas Propagat. Mag.*, Vol. 43, 100–107, 2001.
29. Harrington, R. F., *Time-harmonic Electromagnetic Fields*, Section 3.5, McGraw-Hill, New York, 1961.
30. Morse, P. M. and H. Feshbach, *Methods of Theoretical Physics*, Part 2, Chapter 13, McGraw-Hill, New York, 1953.
31. GEMS Quick Star Guide: http://www.2comu.com.
32. Yu, W., R. Mittra, T. Su, Y. Liu, and X. Yang, *Parallel Finite Difference Time Domain Method*, Artech House, Massachusetts, Jun. 2006.
33. Yu, W., X. Yang, Y. Liu, R. Mittra, D.-C. Chang, C.-H. Liao, M. Akira, W. Li, and L. Zhao, "New development of parallel conformal FDTD method in computational electromagnetics engineering," *IEEE Antennas Propagat. Mag.*, Vol. 53, 15–41, 2011.